Subrelativistic Alternating Phase Focusing Dielectric Laser Accelerators

Payton Broaddus,[1] Thilo Egenolf,[3] Dylan S. Black,[1] Melanie Murillo,[1] Clarisse Woodahl,[1] Yu Miao,[1] Uwe Niedermayer,[3] Robert L. Byer,[2] Kenneth J. Leedle,[1] and Olav Solgaard[1]

[1]*Department of Electrical Engineering, Stanford University, 350 Serra Mall, Stanford, California 94305-9505, USA*
[2]*Department of Applied Physics, Stanford University, 348 Via Pueblo Mall, Stanford, California 94305-4090, USA*
[3]*Technische Universität Darmstadt, Institut für Teilchenbeschleunigung und Elektromagnetische Felder (TEMF), Schloßgartenstraße 8, 64289 Darmstadt, Germany*

(Received 24 April 2023; revised 3 October 2023; accepted 19 December 2023; published 23 February 2024)

We demonstrate a silicon-based electron accelerator that uses laser optical near fields to both accelerate and confine electrons over extended distances. Two dielectric laser accelerator (DLA) designs were tested, each consisting of two arrays of silicon pillars pumped symmetrically by pulse front tilted laser beams, designed for average acceleration gradients 35 and 50 MeV/m, respectively. The DLAs are designed to act as alternating phase focusing (APF) lattices, where electrons, depending on the electron-laser interaction phase, will alternate between opposing longitudinal and transverse focusing and defocusing forces. By incorporating fractional period drift sections that alter the synchronous phase between $\pm 60°$ off crest, electrons captured in the designed acceleration bucket experience half the peak gradient as average gradient while also experiencing strong confinement forces that enable long interaction lengths. We demonstrate APF accelerators with interaction lengths up to 708 μm and energy gains up to 23.7 ± 1.07 keV FWHM, a 25% increase from starting energy, demonstrating the ability to achieve substantial energy gains with subrelativistic DLA.

DOI: 10.1103/PhysRevLett.132.085001

Dielectric laser accelerators (DLAs) utilize recent advances in semiconductor nanofabrication, high fluence femtosecond lasers, and low emittance electron sources to produce electron accelerators with acceleration gradients 1–2 orders of magnitude higher than conventional copper rf accelerators [1,2]. Key to this technology is the GV/m laser-induced damage threshold of semiconductor materials, which demonstrated acceleration gradients as high as 850 MeV/m for relativistic DLAs and 370 MeV/m for subrelativistic DLAs [3,4]. Leveraging these high gradients over long interaction lengths to produce high energy gains at subrelativistic energies has been difficult due to confinement challenges.

Subrelativistic dual pillar DLAs have the necessary transverse lensing to confine beams within submicron apertures, producing focusing forces equivalent to quadrupole focusing gradients of 1.4 ± 0.1 MT/m [5]. Recently, elements needed to realize fully integrated DLAs have been demonstrated for dual pillar structures in the subrelativistic regime: low energy spread attosecond bunchers, and confinement lattices [6,7]. Central to these successes was the application of alternating phase focusing (APF), originally developed for ion acceleration in the 1950s [8,9] and adapted for DLAs in [10], where the Lorentz force of the accelerating laser mode itself is used for confinement instead of relying on external magnets [11].

In [6], the first APF confinement lattice was demonstrated in DLAs, albeit without acceleration, and in [7], an APF attosecond buncher was demonstrated, producing microbunches compact enough and with low enough energy spread to be injected into an APF DLA. This Letter demonstrates the realization of an accelerating APF DLA, which coherently accelerates and confines electrons over extended distances.

Following [10], APF DLA lattices are designed around a $\hat{z}$ traveling "synchronous electron" in the center $y = 0$ of a symmetric dual drive mode at synchronous phase ϕ_s. Once an injection energy and operating synchronous phase have been selected, the energy ramp is fixed by the structure factor $|e_{1n}|$, incident laser field amplitude E_0, and structure periodicity [12], which follows the Wideroe condition for the first spatial mode, expressed as $\Lambda = \beta_s \lambda_0$, where Λ is the periodicity, β_s is the ratio of the relativistic velocity to the speed of light, and λ_0 is the central wavelength. For a $\hat{x}$ invariant dual pillar DLA powered by two counterpropagating in-phase monochromatic $\hat{z}$ polarized lasers incident from $\pm\hat{y}$, the synchronous electron will gain energy ΔW per period [13],

$$\Delta W(\phi_s) = -q|e_{1n}|E_0\Lambda\cos(\phi_s), \tag{1}$$

where q is the elementary charge. The Lorentz force on a synchronous electron is written as

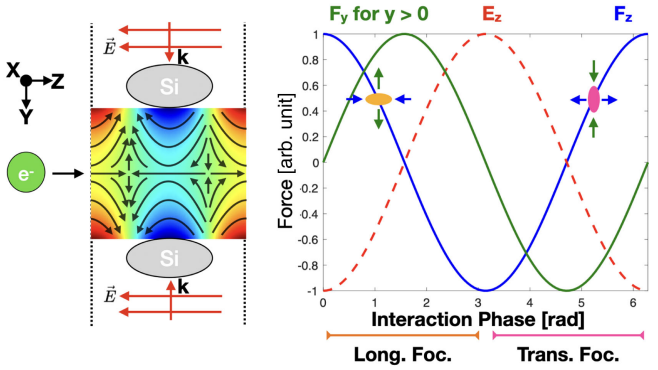

FIG. 1. Left: DLA period with Lorentz force vectors overlaid on electric field $-E_z$ from accelerating mode. Right: E_z and Lorentz forces acting on a reference particle versus interaction phase. Two bunches are drawn at $\phi_s = \pm 60°$, each experiencing half maximum accelerating force F_z and confinement forces of opposite sign in $\hat{y}$ and $\hat{z}$.

$$\vec{F}(\phi_s) = \begin{bmatrix} F_x \\ F_y \\ Fz \end{bmatrix} = \frac{-qc}{\beta\gamma}|e_{1n}|E_0 \begin{bmatrix} 0 \\ \frac{1}{\gamma}\sinh(\Gamma_y y)\sin\phi_s \\ \cosh(\Gamma_y y)\cos\phi_s \end{bmatrix}. \quad (2)$$

γ is the Lorentz factor and $\Gamma_y = ik_y = (2\pi/\lambda_0)\sqrt{(1/\beta_s^2) - 1}$, where k_y is the imaginary (evanescent) wave number for the accelerating first spatial mode. Nonsynchronous electrons experience a Lorentz force $\vec{F}(\phi)$, where the interaction phase ϕ can be expressed as $\phi = \phi_s - \omega_0 \Delta t$ [13]. Here, $\Delta t = t_e - t_s$ represents the difference in arrival time between a nonsynchronous electron and the synchronous electron, denoted by t_e and t_s, respectively, and $\omega_0 = (2\pi c/\lambda_0)$.

As seen in Fig. 1, for synchronous phase $\phi_s \in (0, \pi/2)$, longitudinally defocusing $[(\delta F_z/\delta\phi) > 0]$ and transversely focusing $[F_y(y > 0) < 0]$ forces act on the electrons near the synchronous electron. For synchronous phase $\phi_s \in (-\pi/2, 0)$, the opposite occurs, longitudinal defocusing and transverse focusing forces. The synchronous phase, and thus longitudinal and transverse focusing forces, can be switched via fractional drift sections [10],

$$l_{fd} = (2\pi - \phi_s)\Lambda/\pi, \qquad l_{df} = (\pi - \phi_s)\Lambda/\pi, \quad (3)$$

where l_{fd} switches the forces on electrons near a synchronous reference particle from transversely focusing to transversely defocusing, and l_{df} from transversely defocusing to transversely focusing. By using these fractional drift sections, a properly designed APF DLA can capture electrons with the correct injection phase and transport them in an accelerating bucket over extended distances.

Two dual pillar APF DLA lattice designs were tested, which will be referred to as DLA70 (designed at TU Darmstadt) and DLA100 (designed at Stanford). Both were designed for operation at 1980 nm, 96 keV injection energy and synchronous phase ±60°. Unlike [6], which operated at synchronous phase ±90° without acceleration and with full confinement force, operating at ±60° provides half maximal acceleration and 86% maximal confinement force, a good balance between maximizing both confinement and temporal acceptance and maximizing average gradient [10].

Each had different pillar dimensions, with structure factor $|e_{1n}|$ ranging from 0.68 to 0.78 for DLA70 and 0.37 to 0.46 for DLA100 over the length of the structure, and with optimal dual-drive in-phase peak incident electric field amplitude of 106 and 250 MV/m, respectively. DLA70 and DLA100 had initial acceleration gradients of 70 and 100 MeV/m for on-crest electrons, and 35 and 50 MeV/m for synchronous electrons. The dual pillar geometry of DLA70 exhibited high transparency, suppressing deflecting sinh modes, while DLA100's highly reflective geometry enabled the generation of deflecting sinh modes, which was observed during alignment and was consistent with prior experimental studies [13,14].

DLA70 and DLA100, with channel widths 420 and 400 nm, respectively, were optimized for minimal electron beam sidewall loss [10,15]. The optimization involved iterative cell length selection to minimize the Courant-Snyder $\hat{\beta}_y$ function's maximum, enabling maximum transverse 1D single particle emittance ϵ propagation. For matched beam injection, the beam waist $a(z)$ is $a(z) = \sqrt{\epsilon\hat{\beta}_y(z)}$. Both structures start with $\phi_s = -60°$ for maximal transverse capture.

Figure 2 displays the energy ramps, synchronous phases, and extracted $\hat{\beta}_y$ functions for DLA70 and DLA100 driven at 1980 nm wavelength, and with DLA70 simulated at 106 MV/m and DLA100 at 250 MV/m, the amplitude with best extracted $\hat{\beta}_y$ and a slight sinusoidal phase envelope.

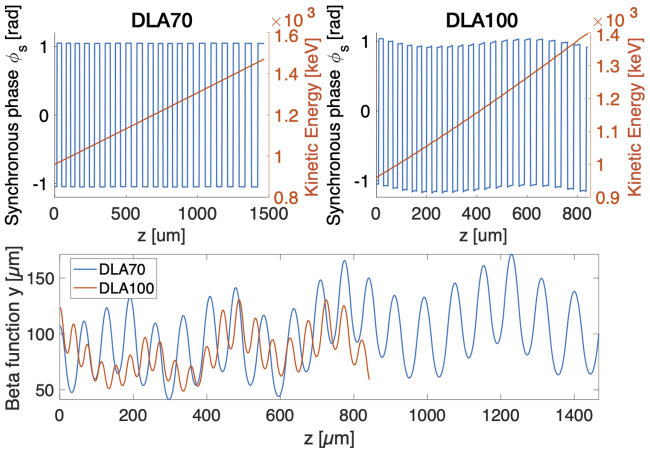

FIG. 2. Synchronous phase and energy (top) and Courant-Snyder $\hat{\beta}_y$ function (bottom) for infinitesimal emittance versus travel distance extracted from DLAtrack6D simulation. The nominal electric field is 106 MV/m for DLA70 and 250 MV/m for DLA100, respectively.

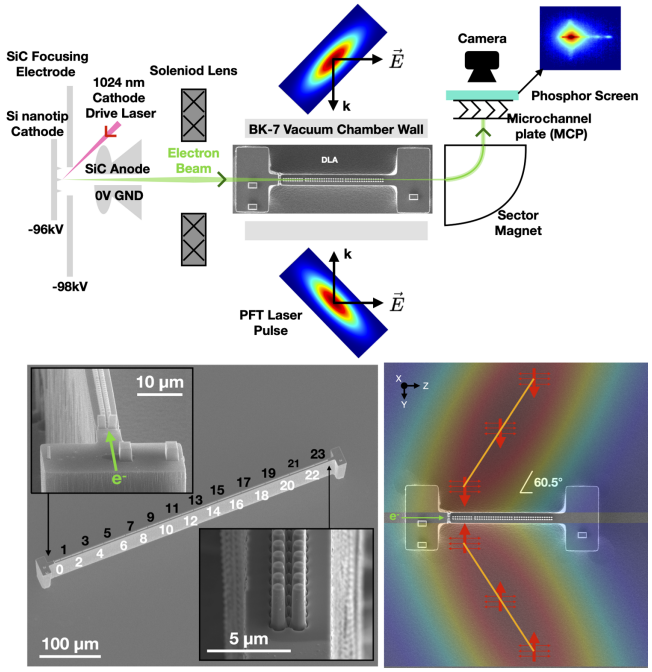

FIG. 3. Top: accelerator system overview. Bottom left: DLA100 476 μm on a 500 μm long mesa. Cells labeled as black are longitudinally focusing and transversely defocusing, while white are longitudinally defocusing and transversely focusing. Bottom right: DLA100 46 μm powered by two $60.5 \pm 0.7°$ incident PFT laser pulses. The orange line shows the electron-laser overlap on the laser pulse as it travels through the structure.

Figure 3 shows the experimental setup; see details on fabrication and optics in the Supplemental Material [16]. The electron source generated 96 keV $\pm$ 23 eV FWHM, 830 ± 100 fs FWHM long electron bunches at a rep rate of 100 kHz, producing ~0.5 electrons per shot with ~100 pm rad transverse normalized emittance in $\hat{x}$ and $\hat{y}$ [17]. Once aligned, the devices were symmetrically pumped by two laser beams, and a sector magnet was used to translate energy gain into horizontal displacement on a microchannel plate (MCP) detector [18].

To achieve full electron-laser interaction with the longest 1469 μm DLA structure, our 100 kHz, 310 fs FWHM (field) optical parametrically amplified laser pulses would have needed to be stretched to 8.4 ps using temporal pulse stretching, assuming a temporal flattop pulse. Laser-induced damage threshold scales inversely to the square root of laser pulse duration in near-infrared (NIR) picosecond laser regime, and similarly unannealed silicon pillars have been destroyed with 310 fs pulsed fields as low as 419 ± 42 MV/m [19,20]. As detailed in the Supplemental Material [16], we employ pulse front tilted (PFT) beams in order to keep the local pulse length short while enabling interaction in long structures at nearly constant amplitude [21–23]. The PFT angle is matched for a $\beta = 0.564$ beam, the average velocity assuming a 24 keV energy gain. Because of subrelativistic energy-velocity scaling, this approach has a maximum field amplitude error of 5% for the longest structures [24].

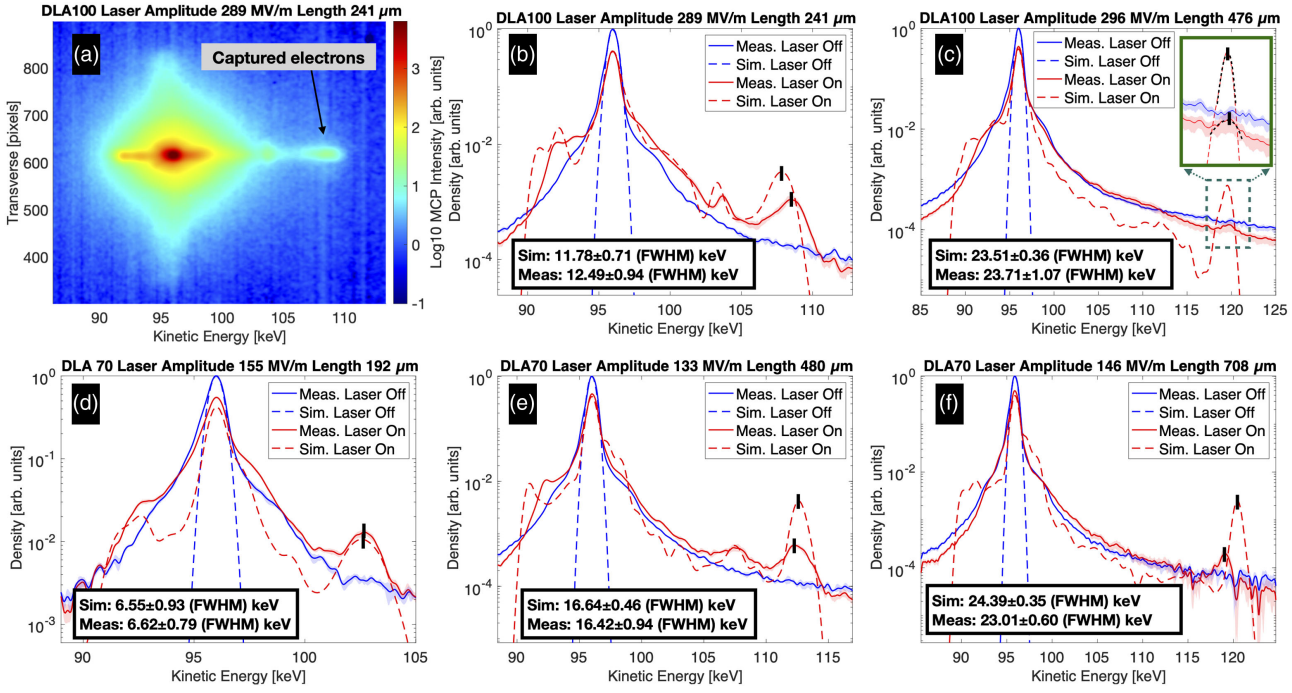

FIG. 4. Simulated and measured laser-on and laser-off spectra for DLA70 and DLA100. (a) Integrated MCP camera image of laser on DLA70 480 μm. Plots in (b)–(f) are obtained by integrating horizontal slices near peak transverse pixel. (b),(c) Simulated and measured DLA100 spectra for laser on and laser off. (d)–(f) Simulated and measured DLA70 spectra for laser on and laser off. A semitransparent overlay on the measured spectra covers the 25%–75% quantile. Experimental parameters in Table I.

TABLE I. DLA70 and DLA100.

	Design params.		Experimental measurements						
DLA type	Length (μm)	Initial gradient (MeV/m)	PFT E_{max} (MV/m)	Wavelength (nm) (sim.)	ΔW (keV) (sim.)	FWHM ΔW (keV) (sim.)	Gradient (MeV/m) (sim.)	Capture (ppm) (sim.)	Capture standard deviation (ppm)
DLA70	192	35	155 ± 17	1980 (1980)	6.62 (6.55)	0.79 (0.93)	34.5 (34.1)	10300 (9620)	5200
DLA70	480	35	133 ± 14	1980 (1980)	16.42 (16.64)	0.94 (0.46)	34.2 (34.7)	449 (1650)	183
DLA70	708	35	146 ± 16	1978 (1980)	23.01 (24.39)	0.6 (0.35)	32.5 (34.4)	76 (658)	61
DLA100	241	50	289 ± 39	1990 (1980)	12.49 (11.76)	0.94 (0.70)	51.8 (48.7)	959 (2315)	445
DLA100	476	50	296 ± 40	1995 (1980)	23.71 (23.51)	1.07 (0.36)	49.8 (49.3)	98 (272)	45

Simulations include this effect as a uniform 5% amplitude and phase error.

Figure 4 shows the measured and simulated (DLAtrack6D [25,26]) MCP spectra for DLA70 and DLA100 of different lengths and peak electric fields for both laser-on and laser-off conditions, with extracted parameters shown in Table I. Laser-on (1980 nm, amplitude as measured in the experiments) and laser-off simulations were performed and simulated, and measured spectra were normalized to their maximum laser-off signal. The simulated and measured spectra [Figs. 4(b)–4(f)] all show similar features: laser-on peak depletion at 96 keV, an asymmetric shoulder modulation, and a captured electron peak, denoted by a black dash marker, with some discrepancy in total count for each feature. For DLA100 241 μm and DLA70 480 μm, clear subpeaks are also visible at 103.2 keV and at 107.3 keV, respectively.

The electron pulse duration (830 fs FWHM) being longer than the laser pulse duration (330 fs FWHM) results in only a portion of the electron pulse interacting and thus experiencing energy modulation from the laser-on signal. This causes peak depletion for the noninteracting injection energy signal and energy modulation for interacting electrons, which was also observed in all previous measured spectra, e.g., [27]. Unlike a strictly periodic DLA, where the modulation is symmetric due to uniform injection sampling of sinusoidal energy gain [Eq. (1)], long multisegment APF DLAs result in an asymmetric signal according to the designed acceleration ramp, seen in both measured and simulated spectra.

APF DLAs ideally should have a prebuncher, which would introduce electrons with the correct injection phase (−60°) with optimal laser amplitude, thus resulting in larger acceleration peak than seen in Fig. 4 [28]. In this experiment, there is no prebuncher, and the 830 fs FWHM electron pulse duration, compared to the laser's 330 fs, results in electrons sampling all laser amplitudes with an approximately uniform injection phase distribution. This complicates attributing any feature, such as the 2–3 keV deceleration shoulder common to all spectra, to a specific injection electron phase space or specific laser amplitude. The exception is the designed acceleration peak, which appears at or above the optimal field and with transverse emittance and injection phase within the accelerator's acceptance (i.e., dynamic aperture). See Supplemental Material for phase space evolution [16].

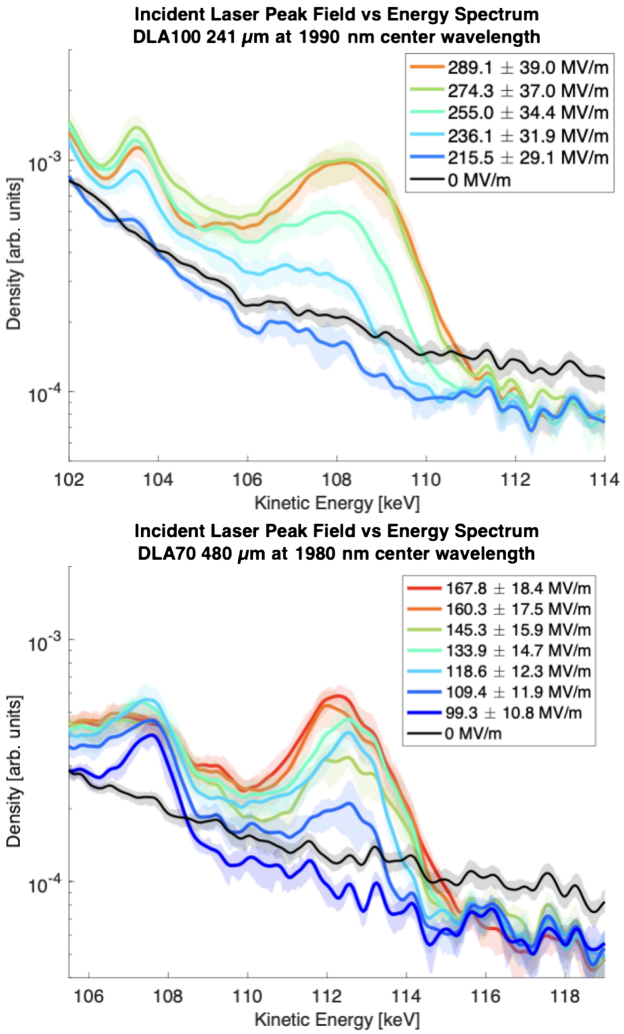

FIG. 5. Measured laser-on spectra for DLA70 and DLA100 with different peak electric fields. DLA70 and DLA100 operate optimally at peak electric field of 106 and 250 MV/m, respectively. A semitransparent overlay on the measured spectra covers the 25%–75% quantile.

Figure 5 shows the acceleration spectra for DLA70 and DLA100 with increasing peak PFT electric field amplitude. DLA70 and DLA100 operate optimally with laser fields of 106 and 250 MV/m, respectively. With larger PFT drive field, more optical cycles of electrons interact with optimal or above fields, resulting in a larger capture peak. For DLA70, there is no visible capture peak at 99.3 MV/m and there is a visible capture peak at 109.4 MV/m, with peak increasing with larger PFT maximum fields. Similarly for DLA100, there is no visible capture peak at 215.5 MV/m and there is a visible capture peak at 236.1 MV/m, also showing the same peak scaling, supporting APF operation. The proportion of arriving electrons that reach designed acceleration, or particle capture, is calculated by multiplying the simulated laser-off particle survival and the normalized capture peak from Fig. 4. Captured current can be approximately obtained by multiplying input current (∼8 fA) and capture rate. An upper limit estimate of ∼50–80 pm rad normalized y transverse emittance is extracted from MCP transverse slices; cf. Supplemental Material [16]. This Letter makes no claims on x emittance.

DLA70 produced a larger accelerated population of electrons than DLA100 for similar lengths, and was easier to align. Furthermore, the DLA100 476 μm structure only worked at a longer wavelength of 1995 nm than designed 1980 nm, and required longer integration time to observe the signal. It is unclear whether the pillar geometry, higher incident field requirements, or design differences resulted in this. Minor dual-drive phase differences generate sinh deflection forces, suppressed by highly transparent pillars in DLA70, but potentially resulting in significant sidewall losses in DLA100.

In conclusion, we demonstrate a subrelativistic DLA architecture that enables extended energy gain over hundreds of optical periods, achieved through the capture and confinement of an electron bunch in the optical fields of a moving-bucket linear accelerator. These structures achieve coherent acceleration, i.e., uniform acceleration of a finite phase space volume, as opposed to a simple broadening of the energy spectrum peak. Good agreement between measured and designed energy gain was observed, with reduced measured versus simulated capture rate expected due to 3D defocusing effects intrinsic to finite pillar height DLA and field amplitude error from the pulse front tilted laser. Capture rate can be improved with electron macrobunching and mircobunching, such as the ones shown in [7,10,29], while longer interaction lengths should be possible with SOI-based 3D APF structures [24,30]. Similar results are shown in [31].

The authors wish to acknowledge the entire ACHIP collaboration for their support and guidance, as well as the staff from the Stanford Nanofabrication Facility (SNF) and Stanford Nanofabrication Shared Facilities (SNSF), supported by the National Science Foundation under Grant No. ECCS-2026822. T. E. additionally acknowledges funding by the German Federal Ministry of Education and Research (Grant No. FKZ: 05K22RDC). This work is funded by the Gordon and Betty Moore Foundation (Grant No. GBMF4744).

[1] R. Joel England *et al.*, Dielectric laser accelerators, Rev. Mod. Phys. **86**, 1337 (2014).
[2] Roy Shiloh, Norbert Schönenberger, Yuval Adiv, Ron Ruimy, Aviv Karnieli, Tyler Hughes, R. Joel England, Kenneth James Leedle, Dylan S. Black, Zhexin Zhao, Pietro Musumeci, Robert L. Byer, Ady Arie, Ido Kaminer, and Peter Hommelhoff, Miniature light-driven nanophotonic electron acceleration and control, Adv. Opt. Photonics **14**, 862 (2022).
[3] Kenneth J. Leedle, R. Fabian Pease, Robert L. Byer, and James S. Harris, Dielectric laser acceleration of sub-100 keV electrons with silicon dual-pillar grating structures, Opt. Lett. **40**, 4344 (2015).
[4] D. Cesar *et al.*, High-field nonlinear optical response and phase control in a dielectric laser accelerator, Commun. Phys. **1**, 46 (2018).
[5] Dylan S. Black, Kenneth J. Leedle, Yu Miao, Uwe Niedermayer, Robert L. Byer, and Olav Solgaard, Laser-driven electron lensing in silicon microstructures, Phys. Rev. Lett. **122**, 104801 (2019).
[6] Roy Shiloh, J. Illmer, T. Chlouba, P. Yousefi, N. Schönenberger, U. Niedermayer, A. Mittelbach, and P. Hommelhoff, Electron phase-space control in photonic chip-based particle acceleration, Nature (London) **597**, 498 (2021).
[7] Uwe Niedermayer, Dylan S. Black, Kenneth J. Leedle, Yu Miao, Robert L. Byer, and Olav Solgaard, Low-energy-spread attosecond bunching and coherent electron acceleration in dielectric nanostructures, Phys. Rev. Appl. **15**, L021002 (2021).
[8] I. B. Fainberg, Some considerations on high-energy electron accelerators, in *Proceedings of the 1st International Conference on High-Energy Accelerators (HEACC)*, edited by E. Regenstreif (CERN, Geneva, 1956).
[9] P. Lapostolle, APF, Los Alamos Technical Report No. 11601, Los Alamos National Laboratory, 1989.
[10] Uwe Niedermayer, Thilo Egenolf, Oliver Boine-Frankenheim, and Peter Hommelhoff, Alternating-phase focusing for dielectric-laser acceleration, Phys. Rev. Lett. **121**, 214801 (2018).
[11] Thomas P. Wangler, *RF Linear Accelerators* (Wiley-VCH, Weinheim, 2008).
[12] Uwe Niedermayer, Oliver Boine-Frankenheim, and Thilo Egenolf, Designing a dielectric laser accelerator on a chip, J. Phys. Conf. Ser. **874**, 012041 (2017).
[13] Kenneth J. Leedle, Dylan S. Black, Yu Miao, Karel E. Urbanek, Andrew Ceballos, Huiyang Deng, James S. Harris, Olav Solgaard, and Robert L. Byer, Phase-dependent laser acceleration of electrons with symmetrically driven silicon dual pillar gratings, Opt. Lett. **43**, 2181 (2018).
[14] Dylan S. Black, Zhexin Zhao, Kenneth J. Leedle, Yu Miao, Robert L. Byer, Shanhui Fan, and Olav Solgaard, Operating

modes of dual-grating dielectric laser accelerators, Phys. Rev. Accel. Beams **23**, 114001 (2020).
[15] Dylan Black, Spatial and temporal electron beam manipulation with dielectric laser accelerators, Ph.D. thesis, Stanford University, 2022.
[16] See Supplemental Material at http://link.aps.org/supplemental/10.1103/PhysRevLett.132.085001 for technical details for the APF DLA experiments and DLATrack6D simulations.
[17] Kenneth J. Leedle, Uwe Niedermayer, Eric Skär, Karel Urbanek, Yu Miao, Payton Broaddus, Olav Solgaard, and Robert L. Byer, High gradient silicon carbide immersion lens ultrafast electron sources, J. Appl. Phys. **131**, 134501 (2022).
[18] Kenneth J. Leedle, Laser acceleration and deflection of sub-100 keV electrons with silicon dielectric laser accelerator structures, Ph.D. thesis, Stanford University, 2016.
[19] Ken Soong, Particle accelerator on a wafer: Demonstration of electron acceleration and diagnostics with microstructures, Ph.D. thesis, Stanford University, 2014.
[20] Yu Miao, Dylan S. Black, Kenneth J. Leedle, Zhexin Zhao, Huiyang Deng, Andrew Ceballos, Robert L. Byer, James S. Harris, and Olav Solgaard, Surface treatments of dielectric laser accelerators for increased laser-induced damage threshold, Opt. Lett. **45**, 391 (2020).
[21] D. Cesar, J. Maxson, X. Shen, K. P. Wootton, S. Tan, R. J. England, and P. Musumeci, Enhanced energy gain in a dielectric laser accelerator using a tilted pulse front laser, Opt. Express **26**, 29216 (2018).
[22] Y. Wei, M. Ibison, G. Xia, J. D. A. Smith, and C. P. Welsch, Dual-grating dielectric accelerators driven by a pulse-front-tilted laser, Appl. Opt. **56**, 8201 (2017).
[23] D. Cesar, J. Maxson, P. Musumeci, X. Shen, R. J. England, and K. P. Wootton, Optical design for increased interaction length in a high gradient dielectric laser accelerator, Nucl. Instrum. Methods Phys. Res., Sect. A **909**, 252 (2018).
[24] Uwe Niedermayer, Thilo Egenolf, and Oliver Boine-Frankenheim, Three dimensional alternating-phase focusing for dielectric-laser electron accelerators, Phys. Rev. Lett. **125**, 164801 (2020).
[25] Uwe Niedermayer, Thilo Egenolf, and Oliver Boine-Frankenheim, Beam dynamics analysis of dielectric laser acceleration using a fast 6D tracking scheme, Phys. Rev. Accel. Beams **20**, 111302 (2017).
[26] U. Niedermayer *et al.*, Challenges in Simulating Beam Dynamics of Dielectric Laser Acceleration, in *Proceedings of the ICAP 2018* (JACoW Publishing, Geneva, Switzerland, 2019), pp. 120–126, 10.18429/JACoW-ICAP2018-MOPLG01.
[27] E. A. Peralta, K. Soong, R. J. England, E. R. Colby, Z. Wu, B. Montazeri, C. McGuinness, J. McNeur, K. J. Leedle, D. Walz, E. B. Sozer, B. Cowan, B. Schwartz, G. Travish, and R. L. Byer, Demonstration of electron acceleration in a laser-driven dielectric microstructure, Nature (London) **503**, 91 (2013).
[28] Uwe Niedermayer, Electron beam dynamics in dielectric laser accelerators, Habilitation thesis, Technische Universität Darmstadt, 2022.
[29] Zhexin Zhao, Kenneth J. Leedle, Dylan S. Black, Olav Solgaard, Robert L. Byer, and Shanhui Fan, Electron pulse compression with optical beat note, Phys. Rev. Lett. **127**, 164802 (2021).
[30] Uwe Niedermayer, Jan Lautenschläger, Thilo Egenolf, and Oliver Boine-Frankenheim, Design of a scalable integrated nanophotonic electron accelerator on a chip, Phys. Rev. Appl. **16**, 024022 (2021).
[31] Tomáš Chlouba, Roy Shiloh, Stefanie Kraus, Leon Brückner, Julian Litzel, and Peter Hommelhoff, Coherent nanophotonic electron accelerator, Nature (London) **622**, 476 (2023).